ELSEVIER

Earth and Planetary Science Letters 166 (1999) 57–70

EPSL

The generation of gas overpressure in volcanic eruptions

Hélène Massol *, Claude Jaupart

Institut de Physique du Globe de Paris, Laboratoire Dynamique des Systemes Geologique, 4 Place Jussieu-Boite 89, 75252 Paris cedex 05, France

Received 30 July 1998; revised version received 7 December 1998; accepted 14 December 1998

Abstract

Observations of natural eruption products show that different parts of a single magma batch may experience different degassing histories during ascent in a volcanic conduit. In non-explosive eruptions, lava issuing from a volcanic vent may contain overpressured gas bubbles. These important features of volcanic eruptions cannot be accounted for by existing flow models, which rely on simplifying hypotheses for the relationship between pressures in the gas phase and in the bulk flow. Volcanic flows involve highly compressible material which undergoes large viscosity variations as degassing proceeds. We show that these properties may lead to large gas overpressures in erupting lava. The magnitude of this overpressure depends on the initial volatile content of magma and is largest for relatively volatile-poor magmas, due to the extreme viscosity variations at water contents less than 1 wt%. We develop a simple analytical model to illustrate the main features of compressible viscous flows: (1) at any level, gas pressure is larger near the conduit axis than at the walls, (2) gas overpressure is an increasing function of mass discharge rate.

Keywords: viscosity; compressibility; explosive eruptions; magmas; viscous materials; lava flow

1. Introduction

Volcanic eruptions involve the exsolution and expansion of a magmatic gas phase during ascent towards the Earth's surface, implying large variations of the rheological properties and a change of dynamical regime if fragmentation occurs [1]. The various dynamical regimes which may occur out of the volcanic vent are reasonably well-understood, depending on exsolved volatile content, mass discharge rate and conduit dimensions [2]. In contrast, conduit flow models have been less successful in predicting exit conditions at the Earth's surface. This is demonstrated by the fact that a given volcanic system involving magma with given initial volatile contents may lead to different eruption regimes [3–5]. Such complex behaviour shows that the gas content at the vent is not related simply to the total volatile concentration of magma. Various hypotheses have been put forward for this, including gas loss to country rock during ascent [3,6,7], kinetic constraints on degassing [8–12] and the vagaries of the fragmentation process [13]. In most of these studies, flow conditions are specified and the implications for degassing are sought as consequences, whereas, in reality, the conditions for flow and degassing are coupled. As will be discussed below, most flow models rely on simplifying hypotheses which affect the values of gas pressure [14,15].

* Corresponding author. Tel.: +33 14427 3860; Fax: +33 14427 3373; E-mail: massol@ipgp.jussieu.fr

0012-821X/99/$ – see front matter
PII: S0012-821X(98)00277-5

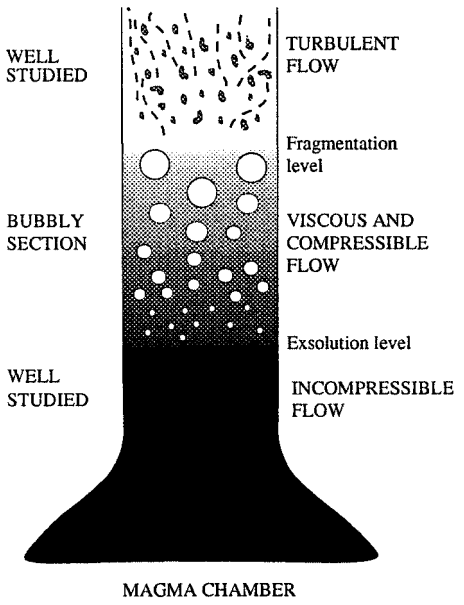

Fig. 1. Schematic representation of the different parts of the volcanic conduit. The intermediate region where bubbles nucleate and expand before fragmentation has not been investigated with the necessary degree of generality.

Fig. 1 summarizes the main processes occurring in a volcanic conduit, emphasizing the 'bubbly' section for which our understanding is poorest: between the exsolution and fragmentation levels. In volatile-poor magmas, fragmentation does not occur, implying that this section extends to the volcanic vent and hence determines physical conditions in the erupting lava. In the bubbly section, the rising volcanic mixture is viscous and experiences large density variations. In most flow models, the governing equations are derived from horizontal averages of the conservation equations [16,1,2], and there is no information on horizontal pressure variations. Disequilibrium effects on bubble expansion are not included, and no gas overpressure is allowed for. The problem is not only one of fundamental physics, but is crucial for understanding constraints brought by petrological and chemical observations on eruption products. Most of these constraints deal with the consequences of degassing, such as the composition of the gas phase, the crystal assemblage present in the erupted magma [4,17], the oxygen isotope ratio and dissolved water content of the melt [18,19]. These observations depend on how gas pressure varies during ascent, which may not be related simply to bulk flow conditions. One effect is that of viscous stresses on bubble expansion, such that gas is overpressured with respect to the melt. In industry, similar effects are encountered in the processing of plastic compounds and have motivated a small number of investigations [20,21]. In a volcanological context, only a few aspects have been discussed [14,22].

The occurrence of gas overpressure in lava has been called upon to explain explosive activity associated with dome growth at Mount Unzen [23] and elsewhere [24]. In a review of many dome eruptions, Newhall and Melson [25] found that key factors for the presence or absence of explosions are the crystal content and water content of the melt, both factors which act strongly on melt viscosity. In a different context, gas overpressure is also indicated by the relatively large dissolved water contents of matrix glass in pumice samples from the recent eruption of Mount Pinatubo [26]. Gas overpressures are also required to drive volatiles out of ascending magma, a process which has received a lot of attention [18,3,27,28,5].

In this paper, we present an analysis of flow in a viscous compressible melt. We develop a rheological model which captures the essential physical ingredients, and derive the corresponding governing equations. In a first section, we determine under which conditions large gas overpressures may be generated and emphasize the fundamental role played by viscosity variations with dissolved water content. We investigate the effects of the various variables involved, such as the initial volatile content of magma and the dimensions of the eruption conduit. In the general case, a complete solution to the compressible flow equations requires a complex numerical algorithm. In a second section, we take a simple set of conditions in order to derive an analytical solution which illustrates the novel dynamical aspects involved. In this calculation, radial pressure variations are taken into account explicitly and solved for as a function of the conduit dimensions. The paper ends with a short discussion of the relevance of the results for understanding volcanic phenomena.

2. Flow model

2.1. Rheology of vesicular magma

Volcanic eruptions involve bubbly magma, for which there is unfortunately no general rheological model valid for all values of the gas volume fraction and for all bubble sizes [29,30]. The key property is obviously compressibility and we focus on it here. The first model for a bubbly liquid was derived by Taylor [31], and was later extended by Prud'homme and Bird [32].

The appropriate constitutive relationship between stress and strain-rate is:

$$\boldsymbol{\tau} = -2\mu\boldsymbol{\epsilon} + \tfrac{2}{3}\mu(\nabla\cdot\vec{v})\boldsymbol{\delta} + P\boldsymbol{\delta} - K(\nabla\cdot\vec{v})\boldsymbol{\delta} \qquad (1)$$

where $\boldsymbol{\tau}$ is the stress tensor, $\boldsymbol{\epsilon}$ the deformation rate tensor, $\boldsymbol{\delta}$ the identity tensor and v the velocity field. There are two viscosity coefficients: the shear viscosity, μ, and the bulk viscosity, K. According to this equation, the flow pressure P_f is the sum of the pressure, P, and the stresses due to bubble expansion:

$$P_\mathrm{f} = P - K(\nabla\cdot\vec{v}) \qquad (2)$$

The bulk viscosity coefficient is [32]:

$$K = \frac{4}{3}\mu_\mathrm{l}\frac{1-\alpha}{\alpha} \qquad (3)$$

where α is the volume fraction of gas and:

$$P = P_\mathrm{g} - 2\frac{\sigma}{a} \qquad (4)$$

where P_g is the pressure of gas inside individual gas bubbles, σ the surface tension, and μ_l the viscosity of the liquid. For negligible surface tension, the thermodynamic pressure for the mixture, P, is equal to the gas pressure. This approximation, valid for bubbles larger than 0.01 mm, is adopted here. Eq. 2 shows that the gas pressure may be higher than the flow pressure.

2.2. Governing equations for ascent in a volcanic conduit

We consider flow in steady-state conditions, which is a reasonable assumption as eruption duration is larger than the ascent time from chamber to surface. We assume that the volcanic conduit is a vertical cylinder of radius a. For an elongated conduit with radius much smaller than its height, we can neglect the horizontal velocity component as in [20,21]. In cylindrical coordinates (r, z), the governing equations for fluid flow are:

$$-\frac{\partial P}{\partial r} + \frac{\partial}{\partial r}\left[\left(K - \frac{2}{3}\mu\right)\frac{\partial w}{\partial z}\right] + \frac{\partial}{\partial z}\left(\mu\frac{\partial w}{\partial r}\right) = 0 \qquad (5)$$

$$-\rho w\frac{\partial w}{\partial z} - \frac{\partial P}{\partial z} + \frac{\mu}{r}\frac{\partial w}{\partial r} + \frac{\partial}{\partial r}\left(\mu\frac{\partial w}{\partial r}\right) + \frac{\partial}{\partial z}\left[\left(K + \frac{4}{3}\mu\right)\frac{\partial w}{\partial z}\right] - \rho g = 0 \qquad (6)$$

$$\frac{\partial(\rho w)}{\partial z} = 0 \qquad (7)$$

where w is the vertical component of velocity. We assume equilibrium degassing conditions and take the following solubility law:

$$x = s\sqrt{P} \qquad (8)$$

where x is the mass fraction of volatiles dissolved in the melt and s a coefficient determined from experiment. For water in silicic melts, we take $s = 4.11\ 10^{-6}\ \mathrm{Pa}^{-1/2}$. Notice that solubility is written in terms of gas pressure and not of bulk flow pressure. Finally, the mixture density is given by [1]:

$$\rho = \left[\frac{1}{\rho_\mathrm{l}}\frac{1-x_\mathrm{s}}{1-x} + \frac{1}{\rho_\mathrm{g}}\left(\frac{x_\mathrm{s}-x}{1-x}\right)\right]^{-1} \qquad (9)$$

with x_s the initial water concentration in the melt, ρ_l magma density and ρ_g gas density.

2.3. Compressibility effects in magma flow

In order to introduce the novel aspects of this model, we momentarily assume that the viscosity coefficients are constant. In this case, Eq. 5 can be integrated with respect to r using boundary condition $w(a, z) = 0$ at the wall:

$$P(r, z) = P(a, z) + \left(K + \frac{1}{3}\mu\right)\frac{\partial w}{\partial z} \qquad (10)$$

where $P(a, z)$ is the pressure at the wall. This shows that a horizontal variation of gas pressure may be generated if the expansion rate, $\partial w/\partial z$, varies across

the conduit. This is indeed the case. At the conduit wall, magma velocity drops to zero and hence the expansion rate also drops to zero. The expansion rate is maximum at the conduit centre where velocity is largest.

2.4. Scaling analysis

In the vertical momentum Eq. 6, we subtract the hydrostatic pressure distribution in a static volatile-free magma column, with density equal to ρ_o everywhere. This introduces $\Delta\rho = (\rho - \rho_o)$. We choose appropriate scales for the variables. A natural pressure scale is buoyancy over the conduit height H, $\Delta P = [\rho_o - \rho_m]gH$, where ρ_m is the average mixture density in the conduit. The density scale is the initial density of the melt, ρ_o. The velocity scale is given by Poiseuille flow in a conduit of radius a. The various scales are therefore: height $= H$; radius $= a$; pressure $= \Delta P = [\rho_o - \rho_m]gH$; viscosity $= \mu_o$; density $= \rho_o$; velocity $= a^2\Delta P/\mu_o H$.

In dimensionless form, the conservation equations are:

$$\frac{\partial P}{\partial r} = \frac{a^2}{H^2}\left\{\frac{\partial}{\partial r}\left[\left(K - \frac{2}{3}\mu\right)\right]\frac{\partial w}{\partial z} + \frac{\partial}{\partial z}\left(\mu\frac{\partial w}{\partial r}\right)\right\} \tag{11}$$

$$\frac{\partial P}{\partial z} = \frac{\mu}{r}\frac{\partial w}{\partial r} + \frac{\partial}{\partial r}\left(\mu\frac{\partial w}{\partial r}\right) - \frac{\rho_o g H}{\Delta P}\Delta\rho + \frac{a^2}{H^2}\left\{\frac{\partial}{\partial z}\left[\left(K + \frac{4}{3}\mu\right)\frac{\partial w}{\partial z}\right]\right\} - \frac{\rho_o a^4 \Delta P}{\mu_o^2 H^2}\rho w\frac{\partial w}{\partial z} \tag{12}$$

This introduces two dimensionless numbers. One is the radius to height ratio, which is typically very small for volcanic conduits. This suggests that radial pressure variations can be neglected. The second dimensionless number may be rewritten as:

$$\frac{\rho_o a^4 \Delta P}{\mu_o^2 H^2} = \frac{a}{H}\frac{a^2\Delta P}{\mu_o H}\frac{\rho_o a}{\mu_o} = \frac{a}{H}Re \tag{13}$$

where *Re* is a Reynolds number. This analysis relies on one important assumption, that the conduit height H is the relevant vertical scale.

3. Bulk flow conditions

3.1. Governing equations and boundary conditions

The flow is laminar below the fragmentation level. According to the scaling analysis, the equations are written to order 0 in parameter a/H:

$$\frac{\partial P}{\partial r} = 0 \tag{14}$$

$$\frac{\partial P}{\partial z} = \frac{\mu}{r}\frac{\partial w}{\partial r} + \frac{\partial}{\partial r}\left(\mu\frac{\partial w}{\partial r}\right) - \frac{\rho_o g H}{\Delta P}\Delta\rho \tag{15}$$

This indicates that pressure is independent of radial coordinate r, and the system of equations reduces to the familiar Poiseuille velocity profile:

$$w = f(z)(1 - r^2) \tag{16}$$

The mass flux G of the eruption is:

$$G = \rho\overline{w}\pi \quad (\rho\overline{w}\pi a^2 \text{ in dimensional form}) \tag{17}$$

where $\overline{w}$ is the horizontal average of velocity. We finally obtain:

$$\frac{dP}{dz} = -\frac{8\mu G}{\pi\rho} - \frac{\rho_o g H}{\Delta P}\Delta\rho \tag{18}$$

Here, the viscosity and density of the bubbly mixture, μ and $\Delta\rho$, vary with height in the conduit following the variation of gas pressure.

In volatile-rich magmas, the volume fraction of gas eventually reaches values that are so large that the bubbly magma becomes unstable and disintegrates into a mixture of magma fragments and gas. The details of this process are outside the scope of the present work. For our purposes, it is sufficient to adopt a simple threshold criterion for fragmentation, such that the gas volume fraction of bubbly magma reaches a critical value of 70%. Above the fragmentation level, flow is turbulent because the viscosity of the volcanic mixture drops to small values. The wall shear stress, τ is equal to:

$$\tau = -\frac{f}{8}\rho\overline{w}^2 \tag{19}$$

where f is a coefficient which depends on conduit roughness. With this definition, the vertical momen-

tum balance is:

$$\frac{\mathrm{d}P}{\mathrm{d}z}\left(1+\frac{\rho_o a^4 \Delta P}{\mu_o^2 H^2}\frac{G^2}{\pi^2}\frac{\mathrm{d}(1/\rho)}{\mathrm{d}P}\right) = -\frac{\rho_o a^3 \Delta P}{\mu_o^2 H}\frac{f\rho\overline{w}^2}{4} - \frac{\rho_o g H}{\Delta P}\Delta\rho \quad (20)$$

For both laminar and turbulent flow, mass conservation is written as:

$$\frac{\mathrm{d}\overline{w}}{\mathrm{d}z} = -\frac{\overline{w}}{\rho}\frac{\mathrm{d}\rho}{\mathrm{d}P}\frac{\mathrm{d}P}{\mathrm{d}z} \quad (21)$$

For boundary conditions, we take a fixed pressure at the base of the conduit, i.e., at the top of the magma reservoir feeding the eruption. This initial pressure is the sum of the lithostatic pressure and of an overpressure ΔP_o. At the top of the conduit, the boundary condition is either one of pressure or one of velocity. If the choking velocity is reached at the vent for pressures larger than the atmospheric value, this is adopted as boundary condition. In this case, at $z = H$, we impose:

$$\overline{w}H = w_c = \left(\frac{\mathrm{d}\rho}{\mathrm{d}P}\right)^{-1/2} \quad (22)$$

3.2. Viscosity coefficients

Magma viscosity depends on the amount of dissolved water. In order to illustrate the key role played by viscosity variations, we consider two different viscosity functions. One is an exponential function [33]:

$$\mu_l = \mu_o \exp[-(x - x_o)\gamma] \quad (23)$$

where μ_o and x_o are the initial magma viscosity and initial water concentration respectively. γ is a positive coefficient which governs viscosity increase with decreasing dissolved water content, fixed at a value of 10^2. This function will be termed 'weak'. Recent experimental data indicate that viscosity varies much more dramatically at small water contents [34] (Fig. 2). Thus, we consider another function, termed 'strong':

$$\log\mu_l = [-3.545 + 0.833\ln(x)] + \frac{9601 - 2368\ln(x)}{T - [195.7 + 32.25\ln(x)]} \quad (24)$$

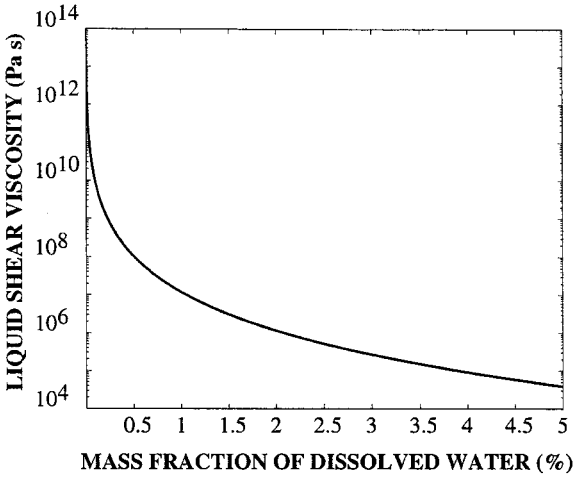

Fig. 2. Liquid viscosity as a function of water content for a leucogranitic melt. Data are taken from [34]. Note the very large viscosity variation when water contents are less than about 1%.

where x is the amount of water dissolved in weight percent and T is in Kelvin.

The shear viscosity of the magma/bubble mixture, μ, depends on bubble shape and on how they deform under shear. This introduces the capillary number:

$$\mathrm{Ca} = \frac{\dot{\gamma}\mu_o b}{\sigma} \quad (25)$$

where $\dot{\gamma}$ is the shear rate and b a typical bubble size. The evolution of bubble shape is difficult to implement in a bulk flow model for a host of reasons. For example, in Poiseuille flow, the shear rate varies across the conduit and drops to zero at the centre. Further, in a volcanic mixture, there is a large range of bubble sizes [35]. We therefore consider two limiting-cases. If bubbles remain spherical, they act to increase the mixture viscosity. In this case, we take an equation drawn from [36]:

$$\mu = \mu_l(1 - \alpha)^{-5/2} \quad (26)$$

where α is the volume fraction of gas. If bubbles get elongated by shear, the mixture viscosity decreases with increasing gas content according to:

$$\mu = \mu_l(1 - \alpha) \quad (27)$$

For the bulk viscosity coefficient, we use Eq. 3.

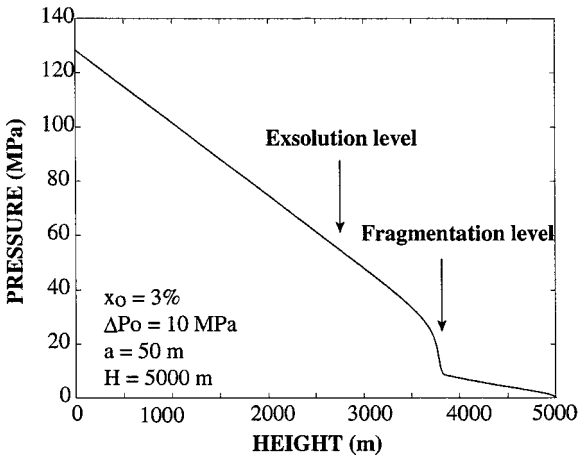

Fig. 3. Bulk flow pressure as a function of height in the conduit using the 'strong' viscosity function from [34]. Other parameters are listed in Table 1.

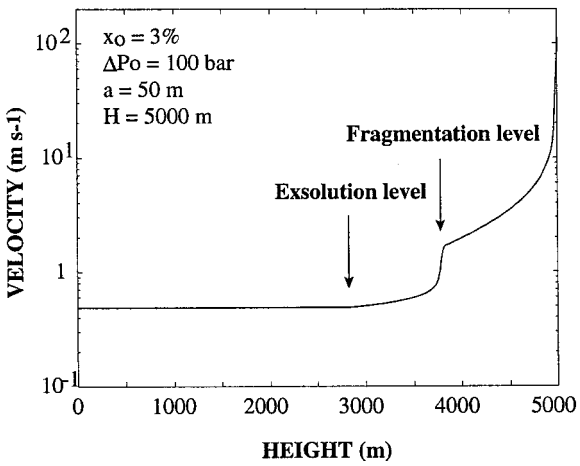

Fig. 4. Vertical velocity as a function of height in the conduit using the 'strong' viscosity function from [34]. Other parameters are listed in Table 1.

3.3. Results

The equations have been integrated with a fourth-order Runge–Kutta scheme. A typical case requires 10^6 space-steps over the conduit height. As magma rises and degasses, the melt viscosity increases dramatically and this generates large variations of flow pressure. Because of expansion, such pressure variations also induce large velocity variations. These changes are very sensitive to the viscosity function used. Results for the 'strong' viscosity function Eq. 24 and undeformed bubbles are given in Figs. 3 and 4. Because of these effects, magma degassing occurs over a very small height range. For the 'weak' viscosity function (Eq. 23), these effects are less marked.

4. Horizontal variations of gas overpressure

We have so far assumed that horizontal pressure variations are negligible, which was justified by the scaling analysis. However, this analysis was based on the choice of H, the conduit height, as the appropriate scale for vertical pressure variations. We have seen that, due to the dependence of viscosity on dissolved water content, flow pressures vary on a much smaller length-scale (see Fig. 3). In this case, there may be large horizontal variations of gas pressure across the conduit, which violates the starting assumption. Our aim is to establish which conditions favour this. We calculate these pressure variations a posteriori, and hence the predicted values of gas pressure may not be accurate.

Eq. 5 can be rewritten as:

$$\frac{\partial P}{\partial r} = \frac{\partial}{\partial r}\left[\left(K + \frac{1}{3}\mu\right)\frac{\partial w}{\partial z}\right] + \frac{\mathrm{d}\mu}{\mathrm{d}z}\frac{\partial w}{\partial r} \tag{28}$$

In the previous calculations, pressure is uniform in the horizontal plane and hence viscosity coefficients do not depend on r. Thus, we can integrate Eq. 28:

$$\Delta P_r = P(0,z) - P(a,z) \approx \left(K + \frac{1}{3}\mu\right)\frac{\partial w}{\partial z}\bigg|_{r=0} + w\frac{\mathrm{d}\mu}{\mathrm{d}z}\bigg|_{r=0} \tag{29}$$

This equation for the horizontal pressure difference is not identical to the earlier one (Eq. 10), which was only valid for constant viscosity coefficients.

The two viscosity functions have different behaviours at small water content. To evaluate the consequences, we consider different initial water concentrations for the melt. For given pressure boundary conditions, such viscosity variations induce variations of flow rate and hence of decompression rate. We wish to separate the effects of the viscosity function and of the decompression rate. Viscosity also depends on melt composition, and we consider two different sets of calculations. In the first one, the initial magma has different water contents but a fixed starting viscosity. Thus, in effect, we are considering different starting magma compositions.

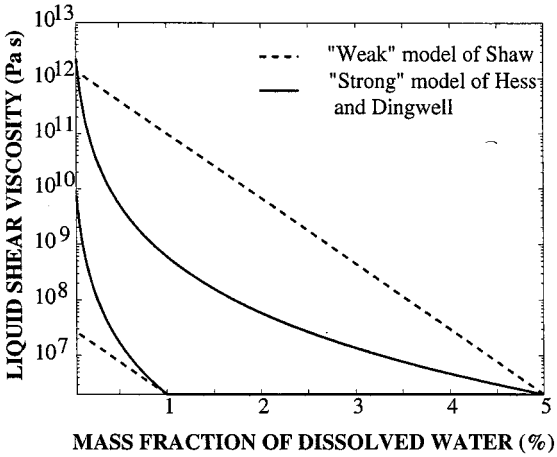

Fig. 5. Melt viscosity as a function of water content for a given starting viscosity. The two different viscosity functions have marked differences in the rate of viscosity variation with decreasing water content. At low initial volatile content, the 'strong' model predicts viscosities which are always higher than those of the 'weak' model. At large initial volatile content, the reverse is true.

The melt viscosity functions are shown in Fig. 5. In a second set of calculations, we consider the same initial magma with different water contents, implying different values of the starting viscosity. In turn, these variations lead to variations of ascent velocity and decompression rate. For clarity, the parameters and assumptions used in the different calculations are listed in Table 1. We calculate the dimensionless magnitude of horizontal pressure variations at the fragmentation level z_f, i.e.:

$$\frac{\Delta P_r(z_f)}{P(z_f)} \tag{30}$$

This is calculated using Eq. 29 and the results of the one-dimensional calculation.

4.1. Variable water content and fixed starting melt viscosity

For each initial water concentration, we consider both the 'strong' and 'weak' viscosity functions. For these different calculations, the mass flux is almost the same because the starting magma viscosity is the same. As shown in Fig. 5, the different initial conditions imply different rates of viscosity variations. In the model, fragmentation occurs at a fixed value of the gas volume fraction, which is achieved for different amounts of degassing depending on the initial water content (Fig. 6).

With decreasing initial water content, the horizontal pressure variation has different behaviours, depending on the viscosity function. With the 'strong' viscosity function, it does not vary significantly for initial water contents larger than 1% because the melt viscosity does not vary much in that range (Figs. 5 and 2). For small water contents, however, it is a very strong function of initial water content because the melt viscosity varies rapidly (Fig. 2). Predicted values for the horizontal pressure contrast are very large. In a few cases, they are so large that they would imply that, at the fragmentation level, the gas pressure is in fact larger than the chamber pressure. This is clearly not self-consistent and emphasizes that the flow model is inadequate. We return to this question below.

The 'weak' viscosity function has interesting behaviour, with the horizontal pressure contrast first

Table 1
Input parameters

Figures	Figs. 3 and 4	Fig. 7	Fig. 8	Figs. 9 and 10
Initial chamber overpressure (ΔP_o), MPa	10	10	10	10
Lithostatic pressure in the chamber, MPa	118	118	118	118
Initial mass fraction of dissolved water, %	3	0.25–4.5	0.25–4.5	0.25–4.5
Conduit radius (a), m	50	50	50	50
Conduit height (H), m	5000	5000	5000	5000
Initial magma density (ρ_o), kg m^{-3}	2400	2400	2400	2400
Bubble shape	Undeformed spheres	Undeformed spheres	Spheres and deformed bubbles	Spheres and deformed bubbles
Viscosity law	'Strong' [34] ($\mu_o = 2 \times 10^6$ Pa s)	'Weak' [33] and 'strong' [34]	'Strong' [34] ($\mu_o = 2 \times 10^6$ Pa s)	'Strong' [34]

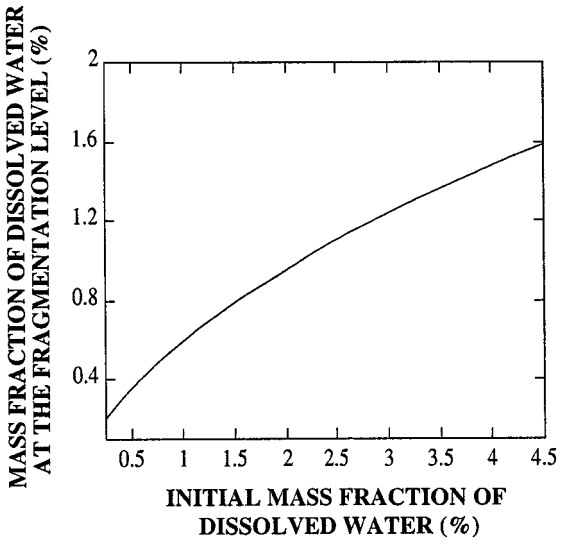

Fig. 6. Mass fraction of dissolved water at the fragmentation level. Parameters for the calculations are listed in Table 1.

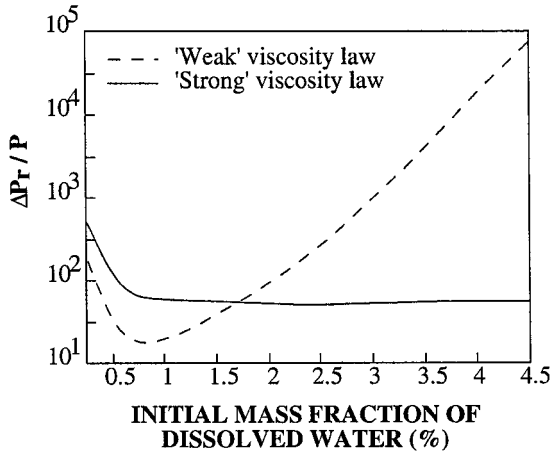

Fig. 7. Predicted magnitude of horizontal pressure variations at the fragmentation level, scaled to the average flow pressure, as a function of initial water content. In these calculations, the starting melt viscosity is the same and the mass flux is almost constant. Two different viscosity functions are used (Fig. 5). These lead to different values of melt viscosity at the fragmentation level. For example, for an initial water concentration of 3%, μ_1 at fragmentation is 2×10^8 Pa s and 4×10^7 Pa s for the weak and strong functions respectively. Parameters for the calculations are listed in Table 1. The very large values obtained in some cases are unrealistic (see text).

decreasing and then increasing with decreasing initial water content (Fig. 7). This is due to the variation of fragmentation pressure and to the fact that the expansion rate increases with decreasing pressure. With large initial water content, fragmentation occurs at relatively large depths, and hence large pressures. In these conditions, it takes large amounts of degassing and hence a large pressure drop to achieve fragmentation. With decreasing initial water content, the fragmentation level moves up and the fragmentation pressure decreases. In this case, fragmentation requires a smaller pressure drop and hence implies a smaller expansion rate. At low initial water content, however, this logic does not apply because one must degas a large fraction of the available water.

Fig. 8 illustrates the effect of deforming bubbles. In this case, the mixture viscosity increases at a smaller rate than in the case of spherical bubbles, and the net effect is a decrease of expansion rate at fragmentation. For the 'strong' viscosity function, horizontal pressure variations are largest for small initial water contents.

4.2. Variable water content and starting melt viscosity

In this set of calculations, we take a fixed starting magma composition and the starting viscosity varies with dissolved water content. This leads to variations of mass discharge rate for given conduit dimensions and pressure boundary conditions. The calculations are carried out for the 'strong' viscosity function, for both deformed and undeformed bubbles. With decreasing water content, the initial melt viscosity increases, and hence the mass discharge rate decreases. In turn, this acts to decrease the expansion rate. Nevertheless, the horizontal pressure variation increases with decreasing initial water content, because of the sharp increase of the rate of viscosity change (Figs. 9 and 10). This emphasizes that significant gas overpressures may occur even in effusive and slow eruptions.

4.3. Discussion

We have shown that the horizontal variation of pressure may be quite large at fragmentation, and that, for the strong viscosity function, it is largest for small initial water contents. The gas overpressure at the centre, $\Delta P_r / P$, is sensitive to the viscosity function for the melt phase, as well as to the behaviour

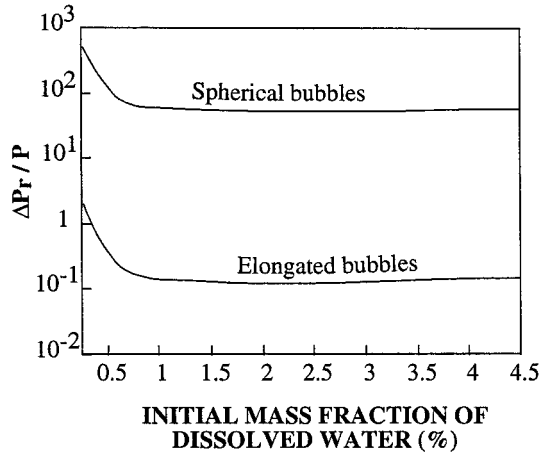

Fig. 8. Predicted magnitude of horizontal pressure variations at the fragmentation level, scaled to the average flow pressure, as a function of initial water content. In these calculations, the starting melt viscosity is the same and the mass flux is almost constant. Two different assumptions for the effect of bubbles on the bulk mixture viscosity are used. Parameters for the calculations are listed in Table 1.

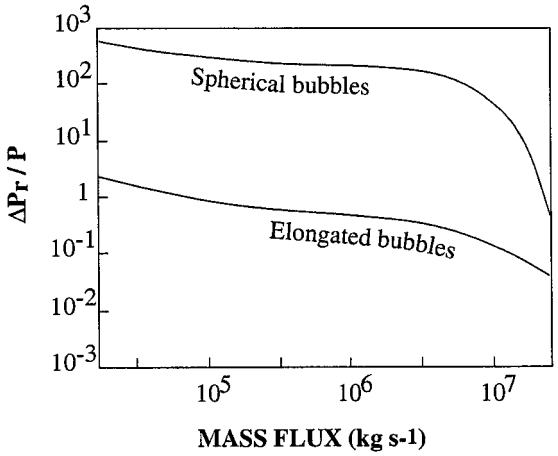

Fig. 10. The magnitude of horizontal pressure variations at the fragmentation level, scaled to the average flow pressure, as a function of eruption mass flux. In these calculations, the starting melt composition is the same and the starting melt viscosity depends strongly on water content as specified by [34]. The mass flux decreases with decreasing water content. Two different functions for the effect of bubbles on the bulk mixture viscosity are used. Parameter values are listed in Table 1.

of bubbles under shear. These results seem to contradict the scaling analysis, which suggested that such horizontal pressure variations were negligible. The cause of this discrepancy is that the scaling analysis relied on a global scale for the decompression rate, estimated as a function of H, the total height of the conduit. We have seen that, when the melt viscosity varies during degassing, pressure varies over a much smaller height range.

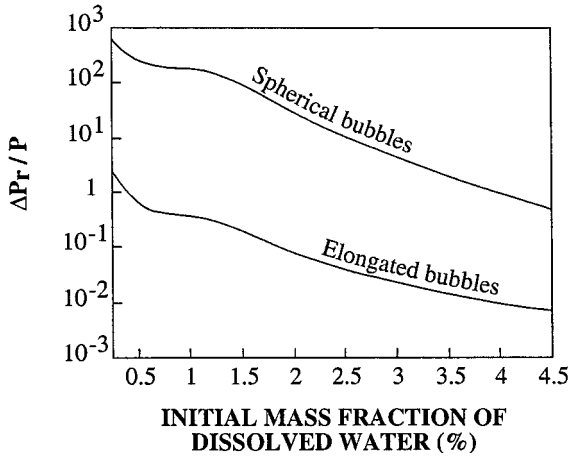

Fig. 9. The magnitude of horizontal pressure variations at the fragmentation level, scaled to the average flow pressure, as a function of initial water content. In these calculations, the starting melt composition is the same and the strong viscosity function is used [34]. With decreasing initial water content, the starting melt viscosity increases and the mass flux decreases. Two different functions for the effect of bubbles on the bulk mixture viscosity are used. Parameter values are listed in Table 1.

Our analysis demonstrates that the assumption of negligible horizontal pressure variations is inappropriate. Significant horizontal pressure variations should drive horizontal flow. One may expect that this will act to reduce the magnitude of the lateral pressure contrast with respect to the present predictions. A proper calculation should allow for large viscosity changes in both vertical and horizontal directions, and requires sophisticated numerical methods in 2-D which are currently being developed. To our knowledge, this problem has never been tackled. In order to illustrate some basic physics of compressible viscous flows, we now present a simple analytical model.

5. A simplified model

We develop an analytical model where gas pressures are allowed to vary in both the vertical and

radial directions. For this, we assume constant viscosity coefficients and constant compressibility. The model does not allow for fragmentation and is designed to emphasize novel flow conditions. It also shows how the various variables come into play. The mixture density varies linearly with pressure:

$$\rho = \rho_o[1 + \beta(P - P_o)] \tag{31}$$

where β is compressibility, P_o and ρ_o are the initial pressure and density in the chamber respectively. If β is small enough ($\approx 10^{-9}\,\mathrm{Pa}^{-1}$) the flow can be considered entirely in a laminar regime. For small conduit radius, small compressibility effects and no viscosity change, following previous studies [20,21], the horizontal velocity components can be neglected. With these assumptions, the conservation equations are:

$$-\frac{\partial P}{\partial r} + \left(K + \frac{1}{3}\mu\right)\frac{\partial}{\partial r}\left(\frac{\partial w}{\partial z}\right) = 0 \tag{32}$$

$$-\frac{\partial P}{\partial z} + \frac{\mu}{r}\frac{\partial}{\partial r}\left(r\frac{\partial w}{\partial r}\right) + \left(K + \frac{4}{3}\mu\right)\frac{\partial^2 w}{\partial z^2} - \rho g = 0 \tag{33}$$

$$\frac{\partial(\rho w)}{\partial z} = 0 \tag{34}$$

With this set of governing equations, the key physical effect, horizontal pressure variations, may be solved for in a self-consistent manner.

5.1. Resolution

Using Eq. 32, we introduce a new variable, called P^*, which depends only on z,

$$P^* = P - \left(K + \frac{1}{3}\mu\right)\frac{\partial w}{\partial z} \tag{35}$$

and rewrite the equations in terms of P^*,

$$-\frac{\mathrm{d}P^*}{\mathrm{d}z} + \frac{\mu}{r}\frac{\partial}{\partial r}\left(r\frac{\partial w}{\partial r}\right) + \mu\frac{\partial^2 w}{\partial z^2} - \rho g = 0 \tag{36}$$

For constant compressibility and no viscosity variation, the conduit height H is the correct scale for z and hence we may use the above scaling analysis with confidence and neglect vertical velocity variations compared to radial ones when $H \gg a$. This was also justified a posteriori. Eq. 36 then reduces to:

$$-\frac{\mathrm{d}P^*}{\mathrm{d}z} + \frac{\mu}{r}\frac{\partial}{\partial r}\left(r\frac{\partial w}{\partial r}\right) - \rho g = 0 \tag{37}$$

In this set of equations, the key aspect is that the mixture density varies as a function of both r and z. For this model, horizontal pressure variations are small and hence we can express density as the sum of a horizontal average and a small deviation $\delta\rho$:

$$\rho = \overline{\rho} + \delta\rho \tag{38}$$

With this assumption, we integrate Eq. 37 with respect to r with the boundary condition $w(a, z) = 0$:

$$w(r, z) = \frac{r^2 - a^2}{4\mu}\left(\frac{\mathrm{d}P^*}{\mathrm{d}z} + \overline{\rho}g\right) \tag{39}$$

This differs from the previous solution because it involves P^* instead of P. We now have four relations for the four variables $\overline{\rho}$, w, P^* and P. The continuity equation is rewritten neglecting the small horizontal density variations:

$$\frac{\partial(\overline{\rho}w)}{\partial z} = 0 \tag{40}$$

Combining these equations, we obtain a differential equation for $\overline{\rho}$, which is solved in Appendix A:

$$\overline{\rho} = A\sqrt{\frac{BH^2}{\Delta P^2}\exp(-2\rho_o g\beta z) + \frac{1}{Ag}} \tag{41}$$

where A and B are integration constants which can be determined with the two boundary conditions at the roof of the chamber and at the vent,

$$\overline{\rho} = \rho_o \text{ at } z = 0, \text{ and } \overline{\rho} = \overline{\rho}_H \text{ at } z = H \tag{42}$$

The novel aspect here is that the exit density is unknown as it depends on the gas pressure at the vent, which itself depends on the mass flux. Both the mass flux and the exit gas pressure must be solved for simultaneously. We write the solution in as a function of the unknown exit density $\overline{\rho}_H$. Using Eq. 41, we obtain:

$$\overline{\rho} = \left\{\frac{\overline{\rho}_H^2 - \rho_o^2\exp(-2\rho_o g\beta H)}{1 - \exp(-2\rho_o g\beta H)}\left[\frac{(\rho_o^2 - \overline{\rho}_H^2)\exp(-2\rho_o g\beta z)}{\overline{\rho}_H^2 - \rho_o^2\exp(-2\rho_o g\beta H)} + 1\right]\right\}^{1/2} \tag{43}$$

We now solve for the exit gas pressure. At the vent, we write the normal stress balance at the top of the vesicular magma column:

$$\tau_{zz}(a, H) = P_a \tag{44}$$

where P_a is the atmospheric pressure. In a general case, this pressure may be larger than the atmospheric value due to the accumulation of lava at the vent. From the definition of P^*:

$$P(r, z) = \overline{P}(z) - \left(K + \frac{1}{3}\mu\right)\frac{d\overline{w}(z)}{dz} + \left(K + \frac{1}{3}\mu\right)\frac{\partial w(r, z)}{\partial z} \tag{45}$$

where $\overline{w}$ is the horizontal average of velocity. Substituting for Eq. 45 in constitutive relation Eq. 1, we deduce that the exit boundary condition Eq. 44 can be written as follows:

$$\overline{P}_H - \left(K + \frac{1}{3}\mu\right)\left.\frac{d\overline{w}}{dz}\right|_H = P_a \tag{46}$$

This boundary condition is rewritten as an equation for the exit density $\overline{\rho}_H$ in Appendix B. This equation must be solved numerically, but an explicit solution is obtained below, which is valid when density variations are very small.

5.2. Results

Once $\overline{\rho}_H$ is determined, pressure is known everywhere in the conduit, from Eq. 45. As shown in Appendix A, the horizontal velocity profile is parabolic, and hence so is the horizontal pressure profile. We verify a posteriori that the hypothesis of small horizontal density variations is valid. For given pressure conditions in the magmatic chamber, we vary the ascent velocities by changing the conduit radius. Fig. 11 shows the maximum gas overpressure ΔP at the vent as a function of mass discharge rate, for two values of compressibility. The overpressure is an increasing function of both compressibility and mass flux. For sufficiently large values of these two variables, the predicted values of ΔP are too large and inconsistent with the starting assumptions.

When $\overline{\rho}$ remains close to the initial density ρ_o, the average density at $z = H$ is expressed as the sum of the initial density ρ_o and perturbative terms:

$$\overline{\rho}_H = \rho_o + a_1\beta + a_2\beta^2 + \ldots \tag{47}$$

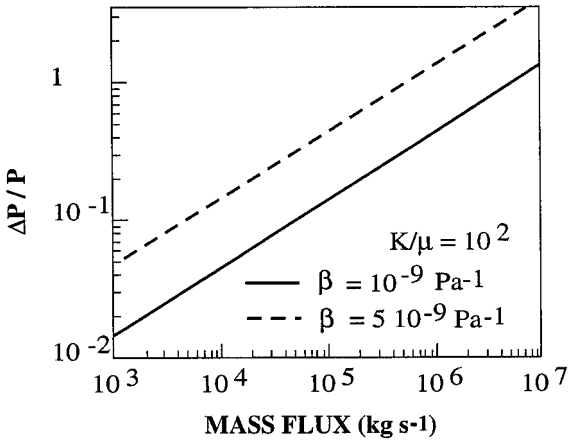

Fig. 11. Gas overpressure at the vent scaled to the pressure at the conduit wall as a function of eruption mass flux. The solution was with the simple analytical model valid for small compressibility. Parameter values are $\mu = 10^7$ Pa s, $\rho_o = 2.4 \times 10^3$ kg m^{-3}, H = 1000 m. The chamber pressure is $P_o = \rho_o g H + \Delta P_o$, with $\Delta P_o = 6.5$ MPa. The eruption mass flux varies as a function of conduit radius a.

At the exit of the conduit:

$$\overline{\rho}_H = \rho_o\left\{1 - \beta\left[P_o - P_a - \beta(P_o - P_a) \times (P_o - P_a - \rho_o g H)\frac{K + \frac{3}{4}\mu}{8\mu}\frac{a^2}{H^2}\right]\right\} \tag{48}$$

We deduce that the exit gas pressure is:

$$\overline{P}_H = P_a + \beta(P_o - P_a)(P_o - P_a - \rho_o g H) \times \frac{K + \frac{4}{3}\mu}{8\mu}\frac{a^2}{H^2} \tag{49}$$

This may be rewritten as follows:

$$\frac{\overline{P}_H - P_a}{P_o - P_a} = \beta(P_o - P_a - \rho_o g H)\frac{K + \frac{4}{3}\mu}{8\mu}\frac{a^2}{H^2} = D \tag{50}$$

where D is a dimensionless number. The maximum gas overpressure is obviously $P_o - P_a$, which would correspond to a rigid mixture allowing no gas expansion, and number D can be interpreted as the fraction of this maximum value which is achieved in the flow. Term $(P_o - P_a - \rho_o g H)$ represents the driving pressure difference for the flow, which acts on the discharge rate and hence on the decompression rate. One may see that the overpressure is proportional to compressibility and that it depends strongly

on conduit radius. For given boundary conditions, the wider the conduit, the larger the flow rate and hence the larger the decompression rate.

For this solution, the mass discharge rate is:

$$Q = \frac{\pi a^4 \rho_o}{8\mu}\left(\frac{P_o - P_a - \rho_o g H}{H} - \frac{\beta(P_o - P_a)}{2}\frac{P_o - P_a}{H} - \frac{P_o - P_a}{H}D\right) \quad (51)$$

The first term corresponds to incompressible flow of liquid with constant density ρ_o. The second term is a correction for variations of liquid density due to non-zero compressibility. The third term introduces the effect of viscous retardation on expansion, and is proportional to dimensionless number D. The net result is a decrease of eruption velocity and hence of discharge rate, because gas expansion does not go to completion. This emphasizes that the eruption mass flux is affected by the details of gas expansion.

6. Discussion and conclusions

The model represents a first step towards a complete physical description of an ascending volatile-bearing magma and ignores several aspects which deserve consideration, which are all related to variations of decompression rates in the flow. Here, we restrict ourselves to one such aspect: during degassing, magma may crystallize microlites. This is a kinetic process, and one may expect that magma rising fast, for example near the conduit axis, leaves little time for microlite nucleation. Near the conduit walls, however, decompression rates are always small, regardless of mass discharge rate and flow regime, and hence there may be sufficient time for microlite growth. The presence of microlites acts to increase magma viscosity and may further enhance gas overpressures. One may envision situations in which only magma lining up the conduit walls bears microlites, in contrast to fast-rising magma at the conduit axis which is microlite-free. The horizontal variation of viscosity which results from this may be very large and may lead to complex flow behaviour.

We have found significant departures from the predictions of simple flow models, which have important consequences for the eruption regime out of the vent and for the behaviour of viscous lava domes. Gas overpressures are large for relatively volatile-poor magmas because magma viscosity varies dramatically at small water contents [34,37]. They may be significant even for small eruption rates and effusive eruptions. This may account for the explosions of lava domes [25] and for abrupt degassing events associated with crack generation within lava domes [28]. Conversely, for volatile-rich magmas which undergo fragmentation early, gas overpressures are not large at the fragmentation level. After fragmentation, however, gas overpressures may be generated within vesicular magma fragments carried by the gaseous flow [13]. Below the fragmentation level, the decompression rate is zero at the conduit walls, and increases towards the conduit centre. Thus, different magma samples erupted simultaneously may have been subjected to different decompression rates and degassing conditions. The large variations of magma viscosity with dissolved water content induce large horizontal variations of gas pressure, which further complicate flow behaviour. These horizontal pressure variations provide a driving force for gas escape through conduit walls [3,6].

Acknowledgements

The manuscript benefited from constructive reviews from R.S.J Sparks and an anonymous reviewer. We also thank Vladimir Lyakhovsky and Oded Navon for fruitful discussions and Cinzia Farnetani for help and comments. ***[AC]***

Appendix A. The average mixture density

Using Eq. 39 and substituting for velocity w in Eq. 40 leads to:

$$\frac{d}{dz}\left[\overline{\rho}\left(\frac{dP^*}{dz} + \overline{\rho}g\right)\right] = 0 \quad (A.1)$$

Integrating this equation leads to:

$$\overline{\rho}\left(\frac{dP^*}{dz} + \overline{\rho}g\right) = A \quad (A.2)$$

where A is a constant. The average vertical velocity is:

$$\overline{w} = \frac{a^2}{8\mu}\left(\frac{dP^*}{dz} + \overline{\rho}g\right) = -\frac{a^2}{8\mu}\frac{A}{\overline{\rho}} \quad (A.3)$$

From Eq. 35, we obtain:

$$\frac{\mathrm{d}P^*}{\mathrm{d}z} = \frac{\mathrm{d}\overline{P}}{\mathrm{d}z} - \left(K + \frac{1}{3}\mu\right)\frac{\mathrm{d}^2\overline{w}}{\mathrm{d}z^2} \tag{A.4}$$

Eq. A.4 can be rewritten in terms of $\overline{\rho}$ only. Eq. A.2 gives an expression for $\mathrm{d}P^*/\mathrm{d}z$ and $\mathrm{d}\overline{P}/\mathrm{d}z$ is calculated using the equation of state with constant compressibility:

$$\frac{\mathrm{d}\overline{P}}{\mathrm{d}z} = \frac{1}{\rho_\mathrm{o}\beta}\frac{\mathrm{d}\overline{\rho}}{\mathrm{d}z} \tag{A.5}$$

Substituting for the various terms of Eq. A.4 leads to:

$$\frac{A}{\overline{\rho}} - \overline{\rho}g - \frac{1}{\rho_\mathrm{o}\beta}\frac{\mathrm{d}\overline{P}}{\mathrm{d}z} + \left(K + \frac{1}{3}\mu\right)\frac{a^2}{8\mu}\frac{\mathrm{d}^2}{\mathrm{d}z^2}\left(\frac{A}{\overline{\rho}}\right) = 0 \tag{A.6}$$

To solve this equation, we change variables and introduce $u = A/\overline{\rho}$:

$$\rho_\mathrm{o}\beta u^3 - A\rho_\mathrm{o}\beta g u + A\frac{\mathrm{d}u}{\mathrm{d}z} + \left(K + \frac{1}{3}\mu\right)\frac{\rho_\mathrm{o}\beta a^2}{8\mu}u^2\frac{\mathrm{d}^2u}{\mathrm{d}z^2} = 0 \tag{A.7}$$

This is made dimensionless using the usual scalings:

$$\frac{\mathrm{d}u}{\mathrm{d}z} + \frac{\beta\Delta P}{A}u^3 - \rho_\mathrm{o}\beta g H u + \frac{K + 1/3\mu}{8\mu}\frac{a^2}{H^2}\frac{\beta\Delta P}{A}\frac{\mathrm{d}^2u}{\mathrm{d}z^2} = 0 \tag{A.8}$$

Three non-dimensional numbers appear:

$$\frac{\beta\Delta P}{A},\quad \rho_\mathrm{o}\beta g H,\quad \frac{a^2}{H^2}\frac{K + 1/3\mu}{8\mu}\frac{\beta\Delta P}{A}$$

The third one is negligible compared to the others when $a \ll H$, and we solve:

$$\frac{\mathrm{d}u}{\mathrm{d}z} + \frac{\beta\Delta P}{A}u^3 - \rho_\mathrm{o}gH\beta u = 0 \tag{A.9}$$

This is a Bernouilli type equation, whose solution is:

$$u = \left(\sqrt{B\exp(-2\rho_\mathrm{o}g\beta z) + \frac{\Delta P}{A\rho_\mathrm{o}gH}}\right)^{-1} \tag{A.10}$$

By definition, $u = A/\overline{\rho}$ and the average mixture density $\overline{\rho}$ is:

$$\overline{\rho} = A\sqrt{\frac{BH^2}{\Delta P^2}\exp(-2\rho_\mathrm{o}g\beta z) + \frac{1}{Ag}} \tag{A.11}$$

Appendix B. Gas pressure and mixture density at the vent

Here, we consider the exit boundary condition, where the gas overpressure is unknown. From Eq. A.3 above:

$$\frac{\mathrm{d}\overline{w}}{\mathrm{d}z} = \frac{a^2A}{8\mu\overline{\rho}^2}\frac{\mathrm{d}\overline{\rho}}{\mathrm{d}z} \tag{B.1}$$

From Eq. 43 of the main text, we have:

$$\left.\frac{\mathrm{d}\overline{\rho}}{\mathrm{d}z}\right|_H = -\frac{\rho_\mathrm{o}g\beta(\rho_\mathrm{o}^2 - \overline{\rho}_H^2)\exp(-2\rho_\mathrm{o}g\beta H)}{\overline{\rho}_H(1 - \exp(-2\rho_\mathrm{o}g\beta H))} \tag{B.2}$$

Using Eq. B.1 and boundary condition Eq. 46, straightforward but tedious manipulations lead to:

$$\overline{\rho}_H^4\left(\frac{1}{\beta\rho_\mathrm{o}} - J\right) + \overline{\rho}_H^3\left(P_\mathrm{o} - \frac{1}{\beta}\right) + p_\mathrm{o}^2J[1 + \exp(-2\rho_\mathrm{o}g\beta H)]\overline{\rho}_H^2 - \rho_\mathrm{o}^4J\exp(-2\rho_\mathrm{o}g\beta H) = 0 \tag{B.3}$$

where quantity J is:

$$J = \frac{\rho_\mathrm{o}g^2\beta a^2\dfrac{K + 1/3\mu}{8\mu}\exp(-2\rho_\mathrm{o}g\beta H)}{(1 - \exp(-2\rho_\mathrm{o}g\beta H))^2} \tag{B.4}$$

This may be solved for $\overline{\rho}_H$.

References

[1] C. Jaupart, S. Tait, 1990, Dynamics of eruptive phenomena, in: Modern Methods in Igneous Petrology, Min. Soc. Am. Rev. 24 (1990) 213–238.

[2] A.W. Woods, The dynamics of explosive volcanic eruptions, Rev. Geophys. 33 (1995) 495–530.

[3] J.C. Eichelberger, C.R. Carrigan, H.R. Westrich, R.H. Price, Non-explosive silicic volcanism, Nature 323 (1986) 598–602.

[4] M.J. Rutherford, P.M. Hill, Magma ascent rates from amphiboles breakdown: an experimental study applied to the 1980–1986 Mount St. Helens eruption, J. Geophys. Res. 98 (1993) 19667–19686.

[5] C. Jaupart, Gas loss from magmas through conduit walls during eruption, in: The Physics of Explosive Volcanic Eruptions, Geol. Soc. London, Spec. Publ. 145 (1998) 75–92.

[6] C. Jaupart, C.J. Allègre, Gas content, eruption rate and instabilities of eruption regime in silicic volcanoes, Earth Planet. Sci. Lett. 102 (1991) 413–429.

[7] A.W. Woods, T. Koyaguchi, Transitions between explosive and effusive eruptions of silicic magmas, Nature 370 (1994) 641–644.

[8] A. Toramaru, Vesiculation process and bubble size distributions in ascending magmas with constant velocities, J. Geophys. Res. 94 (1989) 17523–17542.

[9] C. Klug, K.V. Cashman, Vesiculation of May 18 1980, Mount St. Helens magma, Geology 22 (1994) 468–472.

[10] A.A. Proussevitch, D.L. Sahagian, A.T. Anderson, Dynamics of diffusive bubble growth in magmas: isothermal case, J. Geophys. Res. 98 (1993) 17447–17455.

[11] V.S. Lyakhovsky, S. Hurwitz, O. Navon, Bubble growth in rhyolitic melts: experimental and numerical investigation, Bull. Volcanol. 58 (1996) 19–32.

[12] R.J. Stevenson, N.S. Bagdassarov, C. Romano, Vesiculation processes in a water-rich calc-alkaline obsidian, Earth Planet. Sci. Lett. 146 (1997) 555–571.

[13] E. Kaminski, C. Jaupart, Expansion and quenching of vesicular magma fragments in plinian eruptions, J. Geophys. Res. 102 (1997) 12187–12203.

[14] C. Jaupart, 1992, The eruption and spreading of lava, in: Chaotic Processes in the Geological Sciences, Springer, New York, pp. 175–205.
[15] C. Jaupart, Physical models of volcanic eruptions, Chem. Geol. 128 (1996) 217–227.
[16] L. Wilson, Relationships between pressure, volatile content and ejecta velocity in three types of volcanic explosion, J. Volcanol. Geotherm. Res. 8 (1980) 297–313.
[17] C.H. Geschwind, M.J. Rutherford, Crystallization of microlites during magma ascent: the fluid mechanics of 1980–1986 eruptions at Mount St. Helens, Bull. Volcanol. 57 (1995) 356–370.
[18] S. Taylor, J.C. Eichelberger, H.R. Westrich, Hydrogen isotopic evidence for rhyolitic magma degassing during shallow intrusion and eruption, Nature 306 (1983) 541–545.
[19] S. Newman, S. Epstein, E. Stolper, Water, carbon dioxide, and hydrogen isotopes in glasses from the ca. 1340 A.D. eruption of the Mono Craters, California: constraints on degassing phenomena and initial volatile content, J. Volcanol. Geotherm. Res. 35 (1988) 75–96.
[20] R.K. Prud'homme, T.W. Chapman, R. Bowen, Laminar compressible flow in a tube, Appl. Sci. Res. 43 (1986) 67–74.
[21] H.R. Van Den Berg, C.A. Ten Seldam, P.S. Van Der Gulik, Compressible laminar flow in a capillary, J. Fluid Mech. 246 (1993) 1–20.
[22] S.D.R. Wilson, A mechanism for the lateral transport of gas bubbles in silicic lava rising in a vertical conduit, Earth Planet. Sci. Lett. 156 (1998) 13–18.
[23] H. Sato, T. Fujii, S. Nakada, Crumbling of dacite dome lava and generation of pyroclastic flow at Unzen volcano, Nature 360 (1992) 664–666.
[24] J. Fink, S. Kieffer, Estimate of pyroclastic flow velocities resulting from explosive decompression of lava domes, Nature 363 (1993) 612–615.
[25] C.G. Newhall, W.G. Melson, Explosive activity associated with the growth of volcanic domes, J. Volcanol. Geotherm. Res. 17 (1983) 111–131.
[26] H.R. Westrich, T.M. Gerlach, Magmatic gas source for the stratospheric SO2 cloud from the June 15, 1991, eruption of Mount Pinatubo, Geology 20 (1992) 867–870.
[27] M.V. Stasiuk, J. Barclay, M.R. Carroll, C. Jaupart, J.C. Ratté, R.S.J. Sparks, S.R. Tait, Degassing during magma ascent in the Mule Creek vent (USA), Bull. Volcanol. 58 (1996) 117–130.
[28] R.S.J. Sparks, Causes and consequences of pressurisation in lava dome eruptions, Earth Planet. Sci. Lett. 150 (1997) 177–189.
[29] D.J. Stein, F.J. Spera, Rheology and microstructure of magmatic emulsions: theory and experiments, J. Volcanol. Geotherm. Res. 49 (1992) 157–174.
[30] N.S. Bagdassarov, D.B. Dingwell, Deformation of foamed rhyolites under internal and external stresses: an experimental investigation, Bull. Volcanol. 55 (1993) 147–154.
[31] G.I. Taylor, The two coefficient of viscosity for an incompressible fluid containing air bubbles, Proc. R. Soc. London, Ser. A 226 (1954) 34–39.
[32] R.K. Prud'homme, R.B. Bird, The dilatational properties of suspension of gas bubbles in incompressible Newtonian and non-Newtonian fluids, J. Non-Newtonian Fluid Mech. 3 (1978) 261–279.
[33] H.R. Shaw, Obsidian–H_2O viscosities at 1000 and 2000 bars in the temperature range 700º to 900ºC, J. Geophys. Res. 68 (1963) 6337–6343.
[34] K.U. Hess, D.B. Dingwell, Viscosities of hydrous leucogranitic melts: a non-arrhenian model, Am. Mineral. 81 (1996) 1297–1300.
[35] K.V. Cashman, M.T. Mangan, Physical aspects of magma degassing. 2. Constraints on vesiculation processes from textural studies of eruptive products, Rev. Mineral. 30 (1994) 447–478.
[36] J.O. Sibree, The viscosity of froth, Trans. Faraday Soc. 30 (1934) 325–331.
[37] P. Richet, A.M. Lejeune, F. Holtz, J. Roux, Water and the viscosity of andesite melts, Chem. Geol. 128 (1996) 185–197.